CHALMERS
UNIVERSITY OF TECHNOLOGY

Surface integrity investigations for prediction of fatigue properties after machining of alloy 718

International Journal of Fatigue 144 (2021) 106059

Contents lists available at ScienceDirect

International Journal of Fatigue

journal homepage: www.elsevier.com/locate/ijfatigue

Surface integrity investigations for prediction of fatigue properties after machining of alloy 718

Jonas Holmberg [a,b,*], Anders Wretland [c], Peter Hammersberg [d], Johan Berglund [a], Alfredo Suárez [e], Tomas Beno [b]

[a] RISE Research Institutes of Sweden AB, Argongatan 30, 431 53 Mölndal, Sweden
[b] University West, Production Technology, 461 86 Trollhättan, Sweden
[c] GKN Aerospace Engine System Sweden AB, 461 81 Trollhättan, Sweden
[d] Chalmers University of Technology, 412 96 Gothenburg, Sweden
[e] Tecnalia R&T, Mikeletegi Pasealekua, 7, E-20009 Donostia-San Sebastián, Spain

ARTICLE INFO

Keywords:
Surface integrity
Fatigue prediction
Alloy 718
Machining
Non-conventional machining

ABSTRACT

Fatigue performance is crucial for gas turbine components, and it is greatly affected by the manufacturing processes. Ability to predict the expected fatigue life of a component based on surface integrity has been the objective in this work, enabling new processing methods.

Alloy 718 samples were prepared by different machining setups, evaluated in fatigue testing and surface integrity investigations. These results generated two predictive statistical multi-variate regression models.

The fatigue correlated well with roughness, residual stresses and deformation. The two models showed great potential, which encourages further exploration to fine-tune the procedure for the particular case.

1. Introduction

1.1. Background and objective

New manufacturing technologies which offer improved productivity, are available on the market today for future production of gas turbine components. Many of them allow for higher material removal output but the selection of suitable manufacturing strategies is often difficult. The surface integrity of the final component is of the greatest importance since this determines the fatigue performance [1–3]. Conventional machining methods, like milling, are the common practice today when manufacturing gas turbine parts of superalloys. However, milling of these materials is often time consuming, mainly due to excessive tool wear resulting in short tool life. For this reason non-conventional methods, such as Abrasive Water Jet Machining (AWJM) or wire-Electrical Discharge Machining (W-EDM) have shown potential as suitable alternatives of generating sufficient surface integrity and fatigue performance [4,5].

In order to compare and design the manufacturing route, reliable and capable evaluation methods and procedures for testing and for monitoring need to be established.

There is a lack of established methods for selection of suitable manufacturing strategies that consider surface integrity and fatigue. Fatigue testing is very time consuming as it involves extensive testing and analysis. The major objectives for this work have been to address this knowledge gap by evaluating a methodology for non/semi-destructive prediction of the fatigue crack initiation.

Common for published work within the field of surface integrity and fatigue is that there are no applications where a combined fatigue assessment is done based on topography, stresses, and deformation from the machined surface. Instead, the literature mainly refers to fatigue properties in relation to one process at a time; related to either residual stress or topography. Therefore, a non/semi-destructive predictive tool that utilizes several surface integrity aspects to facilitate the navigation through all design options of the manufacturing process development phase is proposed in this work. The major motive for establishing this assessment tool is to predict the fatigue performance at an early stage when determining the process route for a new component. This will be a useful tool when optimizing the performance of the part when selecting between different manufacturing methods in the industrialization

* Corresponding author at: RISE Research Institutes of Sweden AB, Argongatan 30, 431 22 Mölndal, Sweden.
E-mail addresses: jonas.holmberg@ri.se (J. Holmberg), anders.wretland@gknaerospace.com (A. Wretland), peter.hammersberg@chalmers.se (P. Hammersberg), johan.berglund@ri.se (J. Berglund), alfredo.suarez@tecnalia.com (A. Suárez), tomas.beno@hv.se (T. Beno).

https://doi.org/10.1016/j.ijfatigue.2020.106059
Received 9 September 2020; Received in revised form 16 November 2020; Accepted 17 November 2020
Available online 3 December 2020

phase.

1.2. Machining methods and fatigue

In the present investigation, the assessment method has been developed to cover different manufacturing technologies with the aim of producing a wide range of surface integrity properties. The suggested assessment tool considers the triangulation of topography, surface residual stresses and deformation information. The applied machining methods have been AWJM, W-EDM and conventional milling using cemented carbide tools as well as ultrasonic assisted machining.

1.2.1. Fatigue testing

The fatigue properties of the finished part are a key aspect that need to be considered when defining new manufacturing routes using different machining methods. The fatigue life consists of a crack initiation phase (N_i) and a crack propagation phase (N_p). The former is mainly determined by the surface integrity generated during the finishing steps of the machining process, as shown by Koster et al. [6]. Consequently, the resulting features and defects in the microstructure, such as grain size, texture, porosity or inclusions, has a strong influence on the fatigue properties which was investigated in the literature in a review by Chan for high and ultra-high cycle fatigue of various materials [7]. This review paper also highlighted the lack of existing predictive models that capture the fatigue life.

1.2.2. Conventional milling

The fatigue properties of face milled Inconel 718 were investigated by Wang et al. for a PVD coated carbide tool using different cutting feeds and speeds [8]. It showed that the feed had strong influence; lower feed resulted in higher fatigue strength. The resulting fatigue life increased from 9 to $14x10^4$ cycles as the cutting feed increased from 0.1 to 0.25 mm/tooth. The cutting speed showed less influence and varied instead in the interval of 12–14 $\times$ 10^4 cycles for cutting speed 30–90 m/min. Commonly, all surfaces had tensile stresses ranging from 50 to 400 MPa. Furthermore, Suárez et al. compared the fatigue performance of different machining methods, when machining Alloy 718 [5]. The results showed that milling, especially ultra-sonic assisted milling, resulted in much higher fatigue life than non-conventional methods, AWJM and EDM.

1.2.3. Non-conventional machining

Regarding AWJM process performance, detailed studies has been reported in the literature regarding resulting impact in terms of stresses, topography and fatigue [4,9]. AWJM induce compressive residual stresses in the surface caused by the bombardment of the abrasive particles during the erosive machining. However, some of the abrasives will be embedded into the surface, which has been shown to have a negative impact on the fatigue life [10–13]. Boud et al. showed that both the standoff distance and feed rate influenced surface residual stress, surface topography and fatigue strength when machining aluminum 7475 [14]. The fatigue life was in the interval 3.9–4.9 $\times$ 10^4 cycles when performing bending fatigue testing. Another limiting effect with AWJM is striation and erosion lines in the cut surface, features that could be suppressed by optimizing the traverse cutting speed. These striations can initiate cracks resulting in lower fatigue life compared to a milled surface [15].

The EDM method is a thermal machining process, which induce tensile stresses to the surface and a thin layer of re-melted material. The fatigue properties of Inconel 718 after wire-EDM was compared to a grinded surface by Ayesta et al. [16]. High cycle fatigue bending testing showed similar results for both types of surfaces. However, at higher number of cycles the wire-EDM surface resulted in a slightly lower fatigue strength compared to the ground surface. This was an important observation as both surfaces had similar surface roughness and extension of the heat affected zone, but the residual stresses differed. EDM resulted in tensile stresses of more than 600 MPa while the grinded surface had a high compressive stress of almost (-)400 MPa. This implies that the residual stress levels in the outermost part of the surface, at least in the described case, only had limited influence on the fatigue strength. The result indicated that the properties of the heat affected layer were critical and not the properties of the re-cast layer. This was concluded since the heat affected layer was similar in the described case.

1.3. Fatigue assessment methodology

In the literature, fatigue prediction is mainly categorized into two main groups using simulation tools. The first group relates to prediction of crack nucleation by studies of the stress-strain behavior of the material given a specific damage parameter [17]. The second group predicts the damage on a continuum, computing a damage parameter per cycle [18]. Several other derivatives exist and are well described in the review of Santecchia et al. [19]. The approach in this work is instead to develop a predictive model based on experimentally derived observations of surface integrity and fatigue. A similar approach could not be found in the literature even though several surface integrity parameters have been shown to correlate well with fatigue. E.g. correlation between topography and fatigue is well known and described by many authors [20–22]. However, the relation between fatigue and residual stresses is not that clear, other than the obvious fact that compressive stresses are preferable from a fatigue crack initiation and propagation perspective. Residual stresses are normally measured using X-ray diffraction which is a well-established technique. This method measures the diffraction peak of a specific diffraction plane for the dominating phase in the material. The diffraction peak width withholds additional information of the material state. This is defined as the Full Width Half Maximum (FWHM), which is often mentioned in literature, but it is not used to any great extent within industry. Even though it may possess information directly related the manufacturing process, e.g. by describing the amount of cold work obtained during shot peening [23]. Thus, the FWHM parameter has also shown to correlate with fatigue, e.g. by Zhang et al. who investigated the effect of annealing of a 55NiCrMoV7 steel. The thermal effect from annealing, shown in FWHM and the hardness, had a strong impact on the low cycle fatigue [24].

The correlation between fatigue and FWHM is based on diffraction peak broadening due to the increased dislocation density in the material, which in turn has a major effect on the fatigue properties [25]. The FWHM parameter has proved to be sensitive to variations in the microstructure and the so called stress-strain that is developed during fatigue testing of a surface, shown by Rai et al. for a 9Cr-1Mo steel [26]. It was also shown that FWHM could be used to indicate an initiation of a fatigue fracture on the surface. On a similar topic, Shintani et al. described the relationship between dislocation density and hardness for a cold rolled 304 steel [27]. The results showed that the cold rolling increased the deformation, which increased the dislocation density and the hardness respectively.

The dislocation density was further investigated by Marty et al., who performed modeling for prediction of the yield stress for Inconel 718 [28]. This model predicted the yield stress quiet well, ±50 MPa for a range of 350 MPa. It was further suggested that XRD measurement of the x-ray line broadening is well suited to assess the dislocation density.

In respect to low cycle fatigue, Quesnel et al. studied the influence on FWHM for a low alloyed steel that indicated a decrease of FWHM when the material became softer due to the cyclic fatigue testing [29]. That study further showed that the alterations in the microstructure influenced the initiation of a fatigue failure. Goto et al. showed great potential to correlate the FWHM to fatigue properties of Cr-Mo-V steel grade rotors [30]. Within the off-shore industry similar work was done for stainless steel pipes showing a decrease of FWHM with cyclic fatigue [31–33].

Fatigue damages of a 9Cr-1Mo steel was reported by Rai et al. [26] who observed that the sharp Kα1-Kα2 diffraction peak doublet of the

virgin condition gradually changed into an overlapping, which, in turn, caused a peak broadening. It was also shown how the diffraction peak broadening was affected by various stages of the Low Cycle Fatigue (LCF) cycling. The results showed that FWHM increased with increasing amount of hardening and strain amplitude.

Verification of a part's integrity, including the fatigue performance, is a difficult and time-consuming task. Surface integrity investigations need to be performed thoroughly by evaluating small test pieces of the surface of interest. The literature has shown that individual surface integrity aspects correlate well to fatigue but there are none that consider a combined approach. In this work the focus has been to evaluate a method based on triangulation by utilising non/semi-destructive measurements of the surface integrity to predict the fatigue life. The intension with this work has been to design a framework that can be adapted to other materials or machining methods when a fast assessment of the surface fatigue performance is required. Using this approach is expected to improve the fatigue life prediction since several surface integrity aspects are taken into account.

2. Materials and methods

The work of the present study is a development of the investigations performed by Suarez et al. [5]. In order to develop a better model, an additional data point was added to those investigations, a reference milled surface machined using cemented carbide inserts. This data was added to the prior results to give a more complete set of results to be used in the models.

2.1. Material

The test samples were all taken from the same batch produced from a 6.35 mm thick Alloy 718 plate. The plate was full precipitation hardened by solution annealing at 954 °C for 1 h, followed by water quenching. The precipitation hardening was performed in two stages: (1) First stage at 718 °C for 8 h followed by furnace cooling at 11 °C/hour and (2) second stage held at 621 °C for 18 h. The heat-treated samples had a mean grain size of 7–8 in ASTM scale, 15–32 μm and a hardness of 49 HRC.

The plate was face milled to a thickness of 6 mm, where the fatigue test samples were produced from the cross section. The final sample geometry after the different machining operation was 6x6 mm with a length of 100 mm, adapted to fit the fatigue test setup.

2.2. Machining methods

Three types of milling operations were performed and evaluated in this work; two different milling operations, Conventional, and one ultrasonic (US) milling method. The machining settings are seen in Table 1. The reference milling was carried out with at 32 mm diameter tool equipped with five indexable inserts from Ceratizit. The milling was done using a cutting speed of 45 m/min and feed of 45 mm/min. The other two milling operations were done using a 12 mm solid end mill with four cutting teeth and milling was performed with and without ultrasonic assistance. These two milling operations were carried out at a cutting speed of 80 m/min and a feed of 254 mm/min. The machining settings for these tests are summarized in Table 1.

The two non-conventional machining methods, AWJM and W-EDM, were performed using settings developed for Alloy 718 according to Table 2. These parameters have been developed in order to generate a rough cut of the surface with focus on the cutting speed.

2.3. Fatigue testing

The fatigue testing was performed in a closed loop servo hydraulic testing machine (Instron 8516) using a dynamic load of ±100 kN. Sinusoidal cycles, 3 Hz, were run at room temperature at constant load with an applied load which produces a maximum stress (both tensile and compressive) in the sample of 120% of the yield stress σ_{yp} (yield stress for this material was 1110 MPa), i.e. maximum stress of 1332 MPa and a minimum of 133 MPa. The stress ratio R = Smin/Smax was set to 0.1. Fatigue testing was performed using 4-point bending configuration with dedicated tooling developed with adjustable support and loading points for the test samples. This setup has an interior roll span (t) of 40 mm, an exterior supporting roller span (L) of 80 mm and a sample square section with side (h) of 6x6 mm. This gives a t/h ratio of 6.67 and a L/t ratio of 2, which cause a higher specimen surface stress distribution in the vicinity of the load rollers and secures a fatigue fracture in the designated failure zone. The testing is further described in related work by Suarez et al. [5].

Table 1
Machining settings for manufacturing of the three milled fatigue samples.

Parameter	Reference	Conventional	Ultrasonic	Unit
Machine tool	Kondia A6 3-axis	DMG/Sauer DMU 125P		
Cutting tool				
Supplier	Ceratizit	Fraisa		
Insert designation	XDKT 11T308ER-F40 CTC5235	P8720505 Ø12 r2 Z4, end mill		
Tool holder				
Diameter	32	12		[mm]
No. of teeth	5	4		
Cutting parameters				
Speed, vc	45	80		[m/min]
Feed (f)	45	254		[mm/min]
Feed per tooth (fz)	0.02	0.03		[mm/rev·tooth]
Feed per revolution (fv)	0.1	0.12		[mm/rev]
Radial depth of cut, (a_e)	6 (100% tool immersion)	6 (100% tool immersion)		[mm]
Axial depth of cut, (a_p)	0.17	0.17		[mm]
Ultra Sonic parameters				
Amplitude	–	–	1.5143 (mean)/3 (max)	[μm]
Frequency	–	–	39,610	[Hz]

Table 2
Machining settings used for manufacturing of the AWJM and W-EDM fatigue samples.

Parameter	AWJM	Unit	Parameter	W-EDM	Unit
Operation	Abrasive water jet		Operation	Wire-EDM	
Pressure	350	[MPa]	Wire diameter	0.25	[mm]
Nozzle diameter	0.28	[mm]	Wire material	Brass	
Focusing tube diameter	0.76	[mm]	Dielectric fluid	Deionized water	
Focusing tube length	76	[mm]	Strategy	Rough cutting	
Abrasive mass flow rate	350	[g/min]	Cutting speed	12	[mm/min]
Travers feed rate	20	[mm/min]			

2.4. Examination methods

Evaluation of the surface integrity was done on one machined sample from each of the five different machining methods. All evaluated test samples had the same geometry as the fatigue samples, 6 × 6 × 100 mm.

The surface integrity was evaluated in the center of the middle section of the machined surface of each sample.

2.4.1. Residual stress

Residual stress measurements were performed with X-ray diffraction with a Stresstech G2R XStress 3000 diffractometer equipped with a Mn X-ray tube (λ:0.21031 nm). The modified $\sin^2\chi$ method was used with ±5 tilt (psi) angles (45°…−45°) and the 151.88° diffraction peak. The residual stress was calculated assuming elastic strain theory according to Hook's law and tabulated values for Young's modulus 199.9 MPa as and 0.29 in Poisson's ratio [34,35]. This technique measures the interplanar spacing in the atomic lattices. However, if the lattice is affected by microstructural precipitates, texture or large grains the measured diffraction peak might be distorted and great care needs to be taken when evaluating the measured results. In this case, the samples were aged which has affected the precipitates in the lattice as well as increased the grain size. In order to suppress this influence, a special measurement strategy of oscillating both in tilt, ±5°, and in rotation, ±7°, was adopted. Measurements of residual stress profiles were further performed using layer removal by successive material removal using electro polishing. The electro polishing was done with Struers Movipol equipment and electrolyte A2. All measurements were performed in an accredited laboratory in accordance to the SS-EN 15305:2008 standard [36].

Further, the diffraction peak width, FWHM, holds information of dislocation density. This parameter is calculated as the average value from all 10 measured diffraction peaks for each measurement. In the literature, this parameter is used to describe work hardening [23,37] and was also employed for evaluation in the present investigations.

For evaluation of the diffraction peaks, great care was taken for peak fitting the Kα1 and Kα2. This was done using the methodology with Pearson VII peak fitting and a parabolic background of the Kα1 and Kα2 doublet [38].

2.4.2. Topography

The topography was measured by Coherence Scanning Interferometry with a Sensofar S Neox instrument. The measurements were performed over an 878 × 659 μm surface in the center of the sample at three different positions with a lateral resolution of 0.25 μm. The result was filtered using a spatial median denoise filter with a window size of 5 × 5 points to reduce short wavelength noise and a robust Gaussian filter with a nesting index of 250 μm to remove longer wavelengths.

The topography was evaluated according to the ISO 25178-2:2012 standard. The evaluated parameters include: the arithmetic mean height, Sa; the root mean square height, Sq; the skewness, Ssk; the Kurtosis, Sku; ten point height, S10z, and the developed interfacial area ratio, Sdr [39].

Sa describes the average roughness of the surface, Sq the standard deviation of the height distribution, Ssk represents the degree of bias of the roughness shape (asperity), Sku is a measure of the sharpness of the roughness profile, S10z the average height difference between the 5 highest peaks and 5 deepest pits and Sdr describes the complexity of the surface [39].

2.4.3. Microscopy and hardness testing

The microstructures were evaluated on polished and etched cross sections of the machined surface using light optical microscopy (LOM) and scanning electron microscopy (SEM). The samples for LOM inspection were etched using Kallings solution. The SEM evaluation was done using a Jeol 7800 SEM equipped with a Brucker XFlash 5010 Energy Dispersive Spectroscopy (EDS) detector and a Bruker Electron Back Scatter Diffraction (EBSD) detector.

The hardness was measured with a Qness micro hardness tester, using the Vickers method with a 20 g load. Measurements were performed for three profiles on the polished cross sections for each sample.

2.4.4. Predicting fatigue with correlated predictors

Predicting the fatigue is not straight forward since the surface characteristics are heavily correlated for the studied surfaces in this work. In order to highlight the influence of correlation on the predictability, the relationships were explored using three methods. (1) Ordinary Linear Regression (OLR) models, assuming predictor independence. (2) non-linear models based on Orthogonal Partial Least Square Regression (OPLS) that is not assuming predictor independence. (3) Decision regression Tree models that handle interactions active only within a limited part of the experimental range. In this work, the software JMP Pro 15 was used.

3. Results

In the suggested approach, the aim was to find a high correlation between surface integrity and fatigue by using non/semi-destructive fast evaluation methods. Therefore, the results were divided into non/semi-destructive and destructive evaluations.

3.1. Non/semi-destructive evaluations

3.1.1. Topography

The general appearance of the machined surfaces show great difference in texture, which is more pronounced for the three milled surfaces compared to the more isotropic surfaces generated by AWJM and W-EDM, seen in related work [5]. A subjective ocular inspection shows that the reference surface and the ultrasonic milled surface are quite similar while the conventionally milled surface is comparably rougher. It could further be observed that the AWJM surface has a striation across the machined surface.

The topography was measured at three different locations in the center of the samples, and selected parameters were calculated, presented in Table 3. The range, max – min values, within each sample has been calculated from the three different surface measurements on each sample. This gives information of the variation and repeatability of the measurement procedure. The arithmetic mean value (Sa) shows that the US milled and reference milled surfaces is considerably smoother than the other methods. These results could be compared to the conventionally milled surface that has four times as higher roughness with Sa of 0.8 ± 0.1 μm. This equals to 3x standard deviation of the uncertainty in the roughness measurements.

The two non-conventional methods resulted in the highest Sa of 1.6 ± 0,2 μm for the AWJM surface and 3.4 ± 0,2 μm for the W-EDM surface, which are relatively low values. A similar trend could be observed for the ten-point height parameter (S10z) for the different surfaces. This parameter indicates the lowest global average peak height for the reference milled surface and the US-milled surface, roughly three times better than the conventional method, that in turn, is roughly three times better than AWJM and W-EDM.

The distribution skewness parameter, Ssk, further differentiates the different surfaces. The US-milled and W-EDM surfaces are showing positive Ssk values, which indicate surfaces containing lots of peaks in one plane, while the negative Ssk values of the conventional, reference milled and AWJM surfaces instead indicates surfaces composed of plateaus with fine valleys. The textures further differ between the surfaces where the three milled ones contain texture from the milling tracks. The AWJM texture is defined by the erosion tracks across the surfaces while the W-EDM has an isotropic texture, shown in prior work [5].

3.1.2. Residual stress

The residual stresses and Full Width Half Maximum (FWHM) results show great influence from the different machining methods at both the surface and just below the surface, seen in Fig. 1. The error bars for the stresses represent the deviation from the curve fitting of the measured diffraction peaks.

The surface stresses indicate that the different machining methods

Table 3
Selected topography parameters from ISO25178-2 of the different surfaces.

Parameter Sample	Sq [µm]	Range*	Ssk	Range*	Sku	Range*	Sa [µm]	Range*	S10z [µm]	Range*
AWJM	2.12	0.14	−0.47	0.34	4.36	0.37	1.62	0.12	15.23	3.37
W-EDM	4.25	0.14	0.59	0.16	3.46	1.02	3.38	0.10	20.94	6.25
Mill (insert)										
Reference	0.27	0.01	−0.17	0.57	3.26	0.16	0.21	0.01	1.77	0.29
Mill (solid end mill)										
Ultrasonic	0.25	0.01	0.24	0.16	3.21	0.65	0.20	0.01	2.60	0.51
Conventional	1.04	0.08	−0.61	0.09	2.50	0.19	0.83	0.07	6.11	2.53

* Range: Max-Min values.

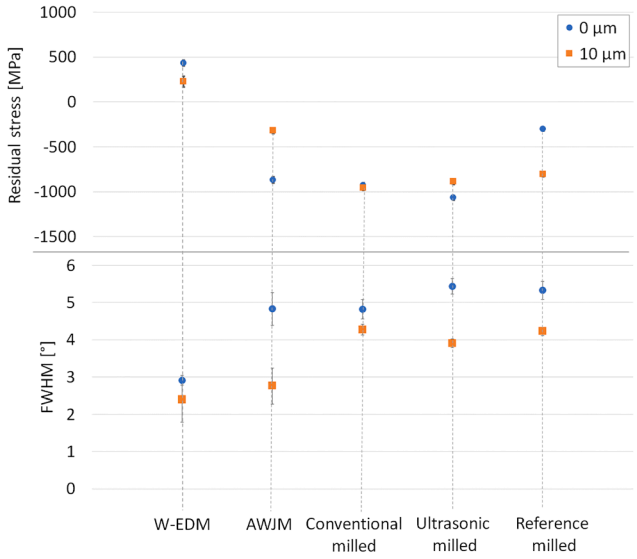

Fig. 1. Surface residual stress results for one sample per machining alternative where the error bars are the variation in the measured data from the curve fitting of diffraction peak data.

can be stratified in three groups. The thermal impact from W-EDM has induced tensile residual stress in the surface, while both the AWJM and the two milled samples with and without US milled samples show quite high compressive residual stresses. The reference milled surface on the other hand show instead moderate compressive stress levels. The impact from ultrasonic milling is highest, which has resulted a 140 MPa higher compressive stress compared to the conventionally milled surface.

The stresses at a depth of 10 µm, show comparably lower values, which is especially observed for the AWJ machined sample. It is further observed that the three milled surfaces have very similar stresses at this depth.

The corresponding FWHM surface values, based on one measurement at one single location, reinforce the difference; they show a clear trend of higher values for the milled surfaces where the US-milled one has resulted in the highest FWHM. The W-EDM has consequently the lowest values implying a low degree of plastic deformation.

The FWHM values at 10 µm depth is lower and the AWJM is showing a comparably lower FWHM than in the surface. It is also seen that conventional milled surface has the highest FWHM at this depth.

3.2. Destructive evaluations

3.2.1. Residual stress

The residual stress profiles also indicate great individual differences depending on the machining methods according to Fig. 2. The error bars and dotted lines represent the deviation from the diffraction peak curve fitting which in some samples increase significantly at depths below 60–90 µm. The reason is due to heavily distorted and multiple peaks detected in the measurements of this material at greater depth, which is most likely effects caused by the precipitation hardening.

The three milling operations have all induced quite high compressive residual stresses in the surface region but with some individual differences. US milling has resulted in highest while the reference milled has comparably lower compressive stress. However, below the surface, at depths greater than 10 µm, all three profiles are very similar. The

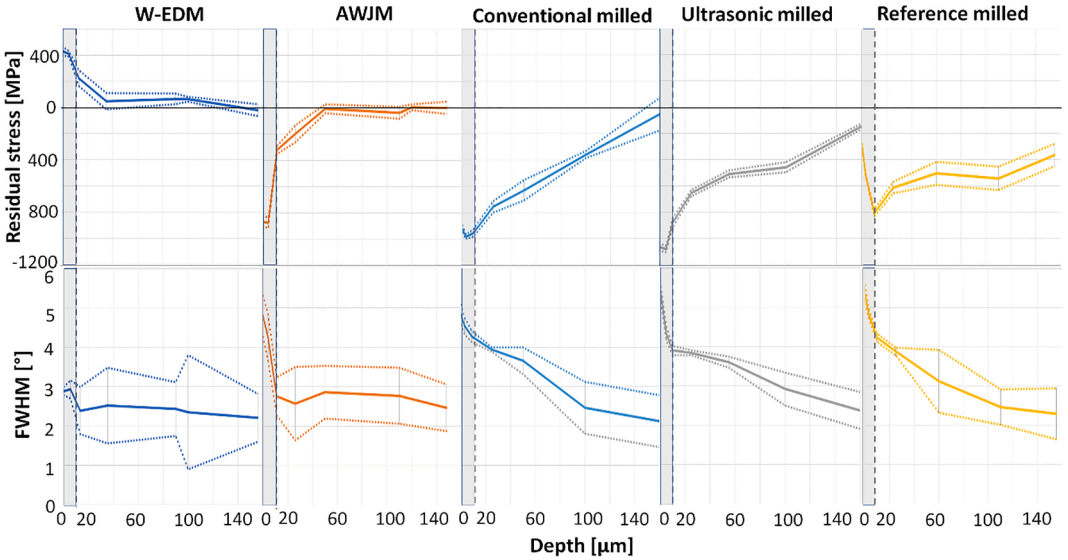

Fig. 2. Residual stress and FWHM profiles evaluated for one sample per machining method.

profiles decrease drastically the first 30 μm and then levels out towards a stress-free state at depths greater than 150 μm. This is comparably deeper relative to the shallow impact for the non-conventional machined ones. Interestingly, a 140 MPa difference is observed between the conventional and US milled surfaces.

The two non-conventionally machined samples show significantly different profiles. AWJM has resulted in a high but shallow, 50 μm, compressive residual stress profile while W-EDM instead induced a high tensile residual stress in the surface and to a depth of 35 μm.

The variation, error bars, with depth is low and constant for W-EDM, AWJM and US milling methods while for the conventional and the reference methods it is higher and increasing.

The corresponding full width half maximum (FWHM) profiles are seen in Fig. 2. It is observed high surface values for the reference and the US milled samples. However, at depths greater than 10 μm the profiles for all milled samples are similar.

AWJM has similar FWHM surface value as the conventionally milled surface but the profile decays rapidly and reaches a core state after 10 μm. The W-EDM sample shows a slightly elevated FWHM at the surface but the core state is reached just below the surface at a depth of 10 μm. However, it should be commented that due to distortion of diffraction peak the FWHM is difficult to assess for greater depths than 50–90 μm, shown by the large variation in the error bars that increases with depth.

3.2.2. Surface fatigue

The results from the four-point bending fatigue testing, No. of cycles to failure (N_f), is presented in Table 4 where the standard deviation is calculated from the 7–10 test samples per machining method. The fatigue strength is lowest for W-EDM and AWJM but interestingly the difference is only marginal.

The milled samples show significantly higher fatigue life where the US milled surface appears to be superior in this test. However, a significantly higher variation was noticed for the US milled sample, but it should be commented that the conventionally and US milled testing were performed only on seven samples and not ten as the other surfaces. The conventionally milled samples have resulted in the lowest fatigue life of the three milled alternatives. Also, worth mentioning is the significantly higher standard deviation for the US milled method, and lower standard deviation for W-EDM. The other three machining alternatives have comparable standard deviations.

3.2.3. Hardness evaluation

Hardness was measured using 3 hardness profiles for each sample and the mean profiles are presented in Fig. 3. The error bars and dotted lines show the standard deviation from the mean values.

The machining impact is clearly shown in these results where the three milling operations have caused a deformation hardening in the surface that is the highest for the US milled surface followed by the reference milled surface. The penetration depth is also following this trend where US-milled sample has the deepest deformation to a depth of 0.2 mm.

In contrast, W-EDM has resulted in a softening of the surface of approximately 70 HV0.02 units and an impact to a depth of 0.16 mm. The AWJM sample shows no hardness impact at all.

The resulting variation in measurements shows similar deviation from the mean profile independently of the depth below the surface.

Table 4
Four-point bending fatigue results for the different machined fatigue samples.

Method	W-EDM	AWJM	Conventional milled	US milled	Reference milled
Nf [# of cycles]	35505 ± 1592	41719 ± 5706	64699 ± 5272	74233 ± 6640	65682 ± 10133

3.2.4. Microstructure evaluation

The deformation was also investigated using SEM-EBSD mapping, seen in Fig. 4. The results show the Mis-Orientation (MO) angles, with the scale set to 0-6° for all samples. MO maps are showing an indirect measurement of the strains within and around different grains.

Generally, for EBSD it is difficult to measure near surface effects due to both sample preparation and the severe deformation that occurs at the outer surface. This has resulted in lack of indexation, which appears as black pixels, caused by the deformation hardening. For this reason, the surface has been marked with a white line for the images of Fig. 4 and it could be observed that, especially for the milled samples, this non-index surface has a typically extension of 10 μm.

These maps clearly illustrate that the deformation differs between the different surfaces, both in depth and mechanisms. The impact depth estimated in the EBSD maps are shown in Table 5. This clearly show the deepest impact for the reference sample of 95 μm followed by the conventional and US milled samples, which had penetration depths of 68 μm and 55 μm respectively. W-EDM has the shallowest impact with less than 5 μm followed by the AWJM which has 14 μm impact depth. Additionally, in Table 5, the total depth impact from hardness measurements are shown which is indicating a deeper impact after the different milling operations.

4. Analysis and discussion

The difference in the resulting surface integrity is a result of the interaction between the machining process and the work piece material. Initially, the fatigue testing was conducted using “as-received” material, resulting in no failure, due to the toughness of the material. Precipitation hardening was performed on the material, which mainly influenced the hardness and distribution of precipitates. The hard particles from the precipitation hardening may alter the surface topography and residual stresses. In related work, it has been shown a slightly higher surface roughness for the hardened material which may be due to the hard particles. However, the residual stresses and FWHM was similar between the material states [4,40,41]. Therefore, low influence of the precipitates acting as abrasives is excepted and the two material states are considered to be comparable in this work.

It has been shown that the depth impact differs greatly between the non-conventional and conventional methods with respect to surface integrity and fatigue. The alteration shows much deeper impact for the conventional methods. This will have an impact on the fatigue as well, but the detailed investigation of its impact requires more testing addressed to investigate the impact of the individual machining method by e.g. different process settings. However, such exploration has not been the focus of this work.

The main objective with this investigation has been to explore the possibilities to develop a framework to predict the fatigue based on triangulation of different measured characteristics of the machined surfaces. The triangulation utilizes two or more points in space to determine an unknown. The goal is a fast and reliable non/semi-destructive surface-based method to take OK/NOK decisions of the fatigue on parts in a development phase.

The literature states that topography, residual stress and deformation are the most important aspects to consider when ensuring high fatigue performance [5,8]. They correlate well individually with the fatigue and may therefore, advance the quality of the prediction even further combined.

The surface integrity investigation in this work shows that the crack initiation phase and propagation phase need to be separated. All studied machining processes resulted in superficial surface deformation with great impact on residual stress, which influence crack initiation. The surface state is characterized by topography, residual stresses and deformation (FWHM). The crack propagation, on the other hand, is related to the sub-surface characteristics monitored also with, residual stress and FWHM, respectively. Results show a severely superficially

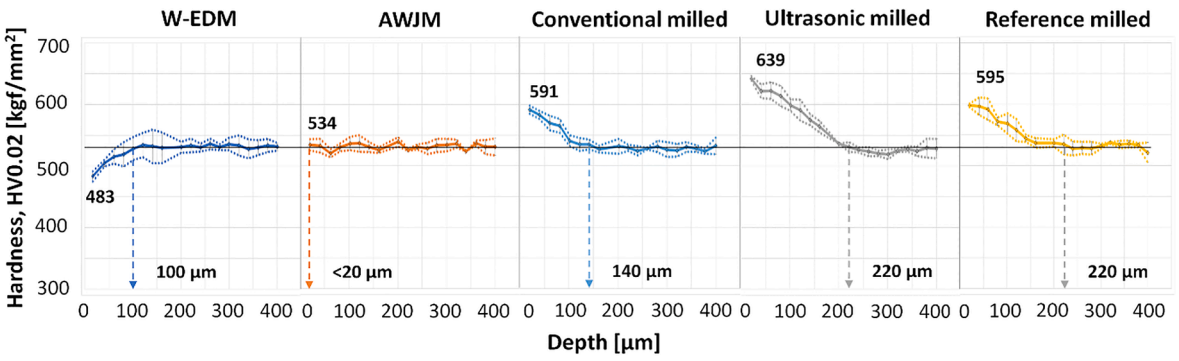

Fig. 3. Hardness profiles for the machined fatigue samples. The surface hardness and impact depth are presented in numbers.

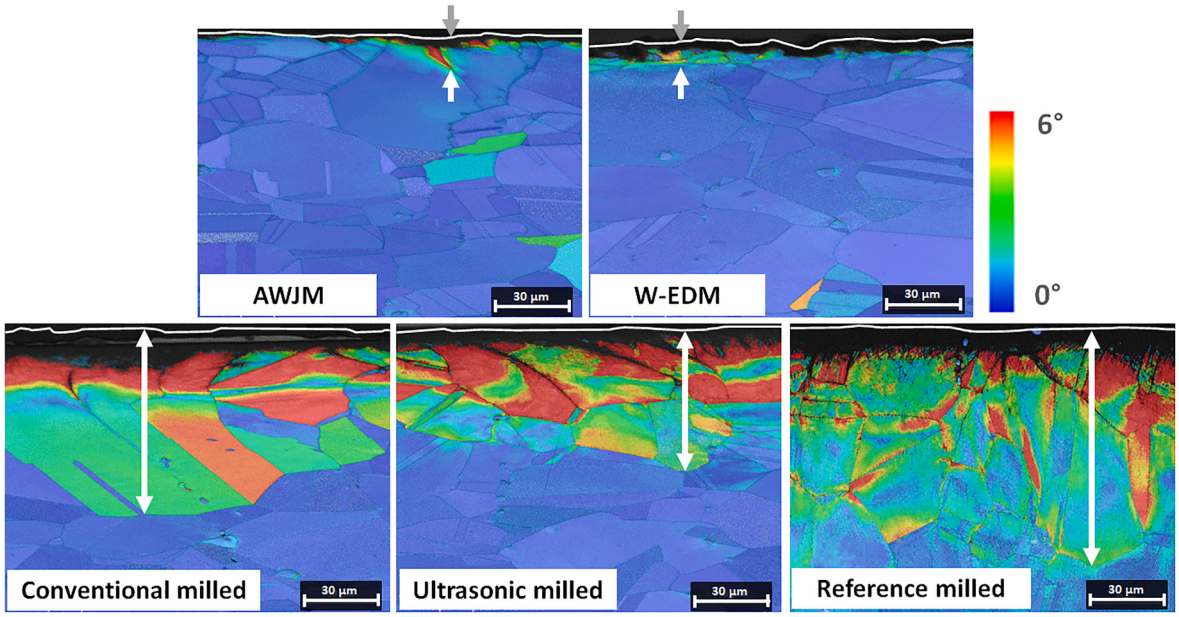

Fig. 4. Misorientation maps in x800 magnification for the different machined fatigue samples. The white arrows indicated the impact depth.

Table 5
Surface deformation depth measured from EBSD maps of the fatigue samples.

Method	Non-conventional		Milled		
	W-EDM	AWJM	Conventional	US	Reference
Surface affected depth [µm]	5	14	68	55	95
Total impact depth [µm]	100	<20	140	220	220

affected 10 µm layer for all surfaces, below which residual stresses and FWHM profiles smoothly decay.

4.1. Correlation between single characteristics

The texture in all surfaces vary, and the milled ones are much smoother than the non-conventionally machined ones. Topography shows the strongest correlation with fatigue, see Fig. 5, which is in agreement with others [42]. Of the topography characteristics, S10z has the strongest correlation with fatigue life indicated by higher degree of R^2 (goodness of fit). S10z is the distance between the five highest peaks and the five lowest valleys. S10z captures, in contrast to Sa (the average height over the measured area), the higher variability in the topography of the AWJM surface better, which correlates with local stress intensities. S10z correlate with the fatigue for all surfaces except the Reference milled surface. It has a similar S10z value as the US milled surface, but there is a slight difference in fatigue. The higher fatigue for smoother surface is exemplified with the difference between US-milled and conventional milled surfaces. It implies different crack initiation mechanisms.

The residual stresses are often mentioned in the literature as a key aspect related to fatigue. The resulting residual stresses also differentiates the machining operations. Fig. 6 display the fatigue versus residual stresses and FWHM, respectively.

As expected, an increasing compressive residual stress increases the number of cycles to failure, which assumes a similar crack propagation phase for these test samples. However, both the AWJM and the reference milled samples deviate from the general trend of a linear relationship between residual stresses and fatigue. Despite the relatively high compressive stresses on the surface −900 MPa, the fatigue life is remarkedly lower. The reference sample show the opposite deviation: higher fatigue than the compressive stresses predict. The deviation for the AWJM on the surface measurements are also confirmed with the FWHM measurements, but not for the reference sample. One plausible explanation for the low fatigue performance is due to the embedded abrasive particles in the surface that resulted in low fatigue performance, shown by several authors [10–12]. This was also confirmed with SEM investigations of the AWJM sample, not presented, which reveal

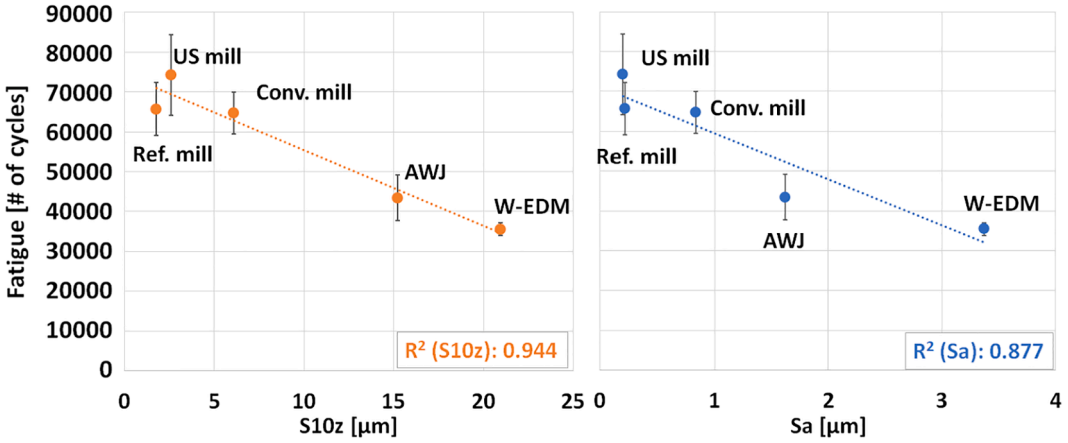

Fig. 5. Surface topography parameters Sa and S10z versus Fatigue for the different machined surfaces.

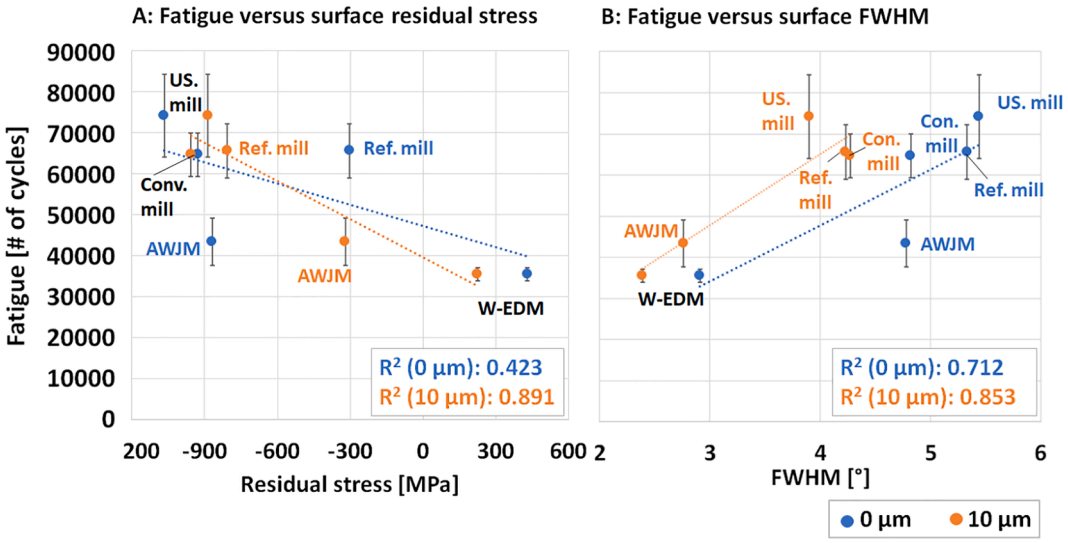

Fig. 6. Fatigue versus residual stresses (A) and FWHM (B) at the surface and at 10 µm below the surface for the different machined surfaces.

embedded abrasive particles, sizes of 2–60 µm. This will greatly affect the early crack initiation due to local stress concentrations, as suggested by Rivero et al. [13]. This imply that S10z might be the better measure, since it captures the local surface variation better, whereas the residual stress is averaged over larger areas missing the relatively small local stress concentrations.

The W-EDM resulted in lowest fatigue performance, which agrees with the study by Ayesta et al. who compared the fatigue strength of wire-EDM and grinding [16]. Interestingly, the number of cycles to failure for W-EDM were in the same range as the AWJM samples despite the difference in tensile and compressive stresses. It confirms that the residual stress measurements, when averaged over a large area, are less correlated with the fatigue relative the effect of the induced cracks from the grinding process, similar to the effect of embedded abrasives from the AWJM process.

The results for the conventional and reference milled samples exemplifies the need to separate the crack initiation from the crack propagation. Both methods show similar fatigue, but the surface residual stresses differ greatly, −1100 MPa for the conventionally milled and −300 MPa for the reference milled. However, at depths below 10 µm, the profiles are very similar, seen in Fig. 2. The US milled sample show on the other hand the highest surface stresses of all samples but not at 10 µm depth where instead the conventional milled surface has the highest compressive stress.

Fig. 6 B shows that FWHM is correlated with fatigue, increasing FWHM with fatigue life, to a higher degree than surface residual stresses. FWHM is an indirect measure of surface deformation that is an effective assessment of fatigue, which has been shown in several publications [22–26]. As with the residual stresses, AWJM deviates from the trend for the surface measurement but not for the sub-surface data.

Summarizing the surface integrity results it can be concluded that all three of the suggested parameters; surface residual stress [MPa], surface FWHM [°] and S10z [µm], individually show great potential to predict No. of cycles to failure [#] both from non-destructively collected surface data and even better with semi-destructive sub-surface data, at depth of 10 µm.

4.2. *Multiparameter predictive modelling*

Statistical evaluation of the pairwise correlations between the surface and sub-surface characteristics are shown in Table 6. There is a strong correlation between FWHM and S10z, which mean that only one is needed for predictive modeling. The interpretation of the bivariate correlation is when the surface roughness decreases, the deformation increases, and vice versa. This appears to be true for the investigated surfaces, but it might not be general, since these two parameters capture different characteristics of the surface. Together, they might reveal underlying characteristics that advance the understanding of fatigue

Table 6
Correlations between the selected parameters for residual stress, FHWM and S10z at surface and 10 μm depth.

Parameter		Sa [μm]	S10Z [μm]	Residual stress (0 μm) [MPa]	FWHM (0 μm) [°]	Residual stress (10 μm) [MPa]	FWHM (10 μm) [°]
S10Z	[μm]	0,97	1,00	0,59	−0,89	0,95	−0,95
Residual stress (10 μm)	[MPa]	0,96	0,95	0,77	−0,90	1,00	−0,95
FWHM (10 μm)	[°]	−0,89	−0,95	−0,54	0,78	−0,95	1,00
Residual stress (0 μm)	[MPa]	0,74	0,59	1,00	−0,81	0,77	−0,54
FWHM (0 μm)	[°]	−0,98	−0,89	−0,81	1,00	−0,90	0,78
Sa	[μm]	1,00	0,97	0,74	−0,98	0,96	−0,89

behavior even further. For example, post processing of a surface in two steps by shot peening and polishing may result in a low S10z value can still have a high FWHM value. When the bivariate relationship is valid an interesting opportunity opens. Surface data from residual stress measurements will be enough to predict the fatigue.

Since the residual stress characteristics and the topography metrics are correlated, Table 6, means they cannot be used in ordinary least square regression (OLS) analysis that assumes independent regressors. It is therefore of central interest to explore what parameters have the strongest ability to predict the fatigue.

Therefore, two different type of models with the potential to handle correlations are compared to OLS: regression decision tree with bootstrap forest versus partial least square regression, using both the surface and sub-surface data.

A Decision Tree regression model analysis [36] using the Partition platform, in the software JMP Pro, has the potential to explore what parameters explain most of the variation without assuming a global model relationship. The strength with it is that it can be used to explore many regressors at the same time and uncover local interactions. Withholding 25% of the data for validation of the model and using 75% for model training, the 82% of the variation in the validation set can be explained by a decision tree based on these parameters, Fig. 7.

Figs. 7 and 8 visualize the decision tree model based on the sub-surface data on residual stress and FWHM and the topography metric s10z. The splits should be read from the top in Fig. 8. The first split when FWHM at depth of 10 μm (FWHM @ 10 μm) is below or above 3.9, divide the Fatigue in two groups with 39,953 and 66,605 number of cycles on sub-group averages, respectively. The second and third split each sub-group into another pair, ending with a model that can classify this data into four discrete categories. The lower panel in Fig. 8 shows that FWHM at 10 μm depth explains 96% of the variation in the fatigue data and s10z parameter the rest and the variation in residual stress (RS) is correlated with the other.

A Partial Least Square (PLS) regression analysis with the same data catches 97% of the variation in the x's and 81% of the variation in Y, Fig. 9. The PLS-model for fatigue prediction is formulated by equation 1 and the corresponding constants in Table 7 and is how the fatigue life depends on each parameter is visualized in Fig. 10.

$$Fatigue = A \times S10z + B \times RS_{10\mu m} + C \times FWHM_{10\mu m} + D$$

Comparing the actual observation of fatigue life versus predicted fatigue of both models reveals that when the decision tree model are categorizing the data in four distinct classes, is the PLS-model only able to separate the fatigue data on three levels, Figs. 11 and 12. The Decision Tree model is able to separate the machining methods, except conventional and reference method, since the fatigue life for these sub-groups are overlapping, already seen in the fatigue result in Table 4. PLS are overestimating the fatigue life of the AWJM method and cannot separate the three machining methods that give longer fatigue life. The models explain 87% and 81% of the total variation in the fatigue data related to the difference between the machining methods, respectively. The remaining percent of the variation comes from the variation within each machining method.

	R^2	Iterations (N)	No. of splits
Training	0.873	35	3
Validation	0.817	9	

Fig. 7. Resulting R2 values for the training and validation set of the decision tree.

The error in the prediction by Decision Tree model based on the sub-surface characteristics are much lower than PLS. In fact, its worst prediction is better than the best prediction for the other method, see Table 8. However, even if the surface characteristics solely are measured on one representative sample per machining method, preventing estimation of the experimental error within each sub-group, the result is encouraging and promising for further exploration. This analysis shows a potential roadmap for prediction of the fatigue life (No to cycles to failure) based on different surface characteristics and modelling techniques.

The sub-surface FWHM measurements hold most information of the fatigue and adding S10z and residual stresses the prediction becomes even more precise, if the correlation is addressed. It could also be commented that even though the limited amount of observation was used in this work, the models manage to predict the fatigue well. For future studies, a greater amount of observations is required to build a model that predict with higher precision. Such work will also need to focus on studying the robustness of the model where these models will be used as a framework.

In regard to the two models developed, each has its pros and cons. The decision tree model is predicting with high accuracy, but the model basically classifies a new observation into one of the discrete levels identified by the training data. Implying that samples representing more fatigue levels are need for training in order to get distinctive categories with narrower range depending on the application requirements. The proposed alternative is PLS modelling that would allow for a continuous prediction. In this case it was however shown that the PLS modeling resulted in lower discrimination capability than the decision tree model does. The reason is due to the few number of observations used to build this model which make the model sensitive for the quality of the data, that will affect the confidence level of the interpolated predicted value. It is further not recommended to use any of these models for extrapolation, that is using them to predict the fatigue life of surfaces machined with other methods.

The fatigue data that build these models where further only from one load case with the stress ratio of 0.1 and should be refitted when more data is available. The literature indicates that the fatigue testing, high or low cycle, may influence the crack initiation and mechanism greatly [43]. Therefore, as commented before, this model-based prediction is to be considered a framework, based on the fatigue testing performed in this work, that needs further refinement. The developed models in this work aims to be generic in the sense that it could give an indicative measure on the expected fatigue for different surfaces, which are normally tested in 4-point bending. Furthermore, the data used in these models are quite unique, S10z and RS/FWHM at 10 μm depth, and a similar approach has not been found in the literature. It is therefore difficult to validate these models to existing data in the literature.

Finally, the five surfaces used were selected to explore the widest range of the surface integrity properties. However, the models showed

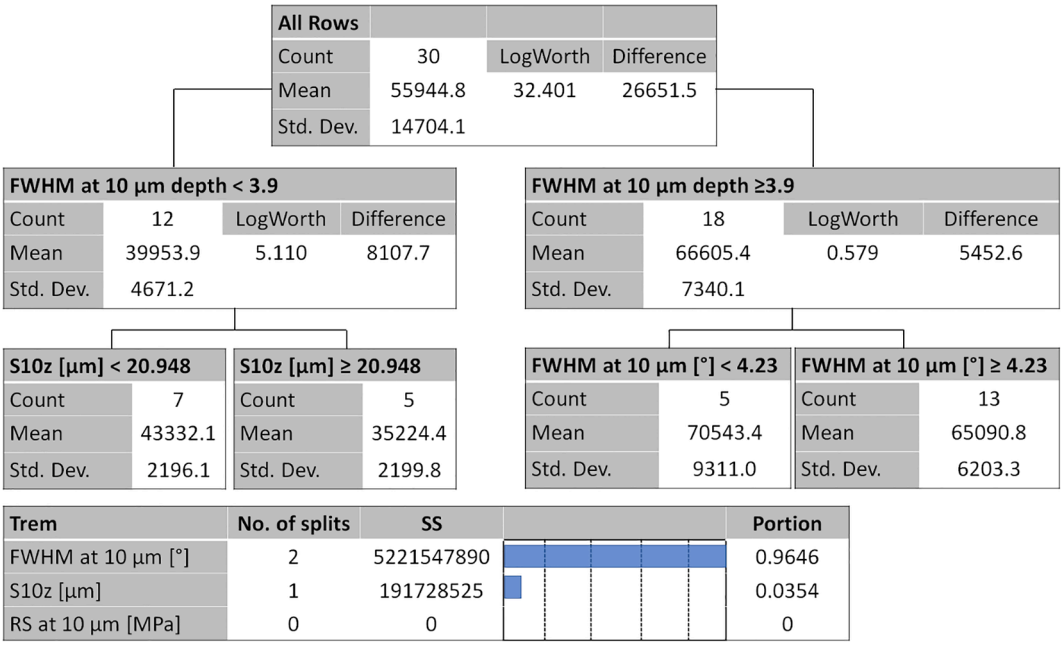

Fig. 8. Decision tree for the model based on the boot strap selected parameters.

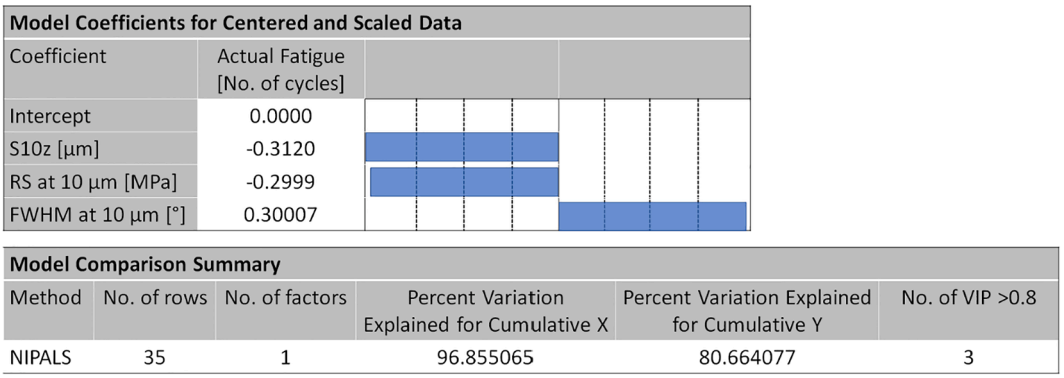

Fig. 9. Parameter for fitting and NIPALS results.

Table 7
Resulting constants for the PLS model.

Constant	A	B	C	D
Value	−661.5	−10.8	6104.5	34821.4

here are sensitive for any variations from the assumed state per observation that are used to generate these models. The promising result urge for additional exploration adding runs with different process parameters settings for each method addressed, alternating the surfaces by means of stresses, FWHM and topography. Such an approach would also further explore the stability of the models by performing refined analysis of the individual samples in order to better incorporate the measured data into the predictive model and potentially find the missing characteristics connected to AWJM surface properties.

5. Conclusions

A combined assessment of the fatigue strength utilizing topography, S10z, residual stress, deformation, and FWHM, advance the resolution and improve reliability which will decrease the need of destructive verification.

The topography for US milling was improved with 76%, Sa and 57%, S10z, compared to the conventionally milled surface but fatigue was only improved 15%, implying a scaling factor.

Strong correlation between surface and subsurface properties of roughness, residual stress, full width half maximum and resulting fatigue was shown.

Topography parameter, S10z, had the strongest linear correlation to the fatigue life as this parameter better captures the surface variations that induce local stress intensity which, in turn, decrease the number of stresses to crack initiation.

Statistical analysis show that through decision tree modeling FWHM at a depth of 10 µm contributes with 96% of the explanation in this tree and only 4% comes from the s10z parameter.

Statistical analysis showed a strong correlation between S10z and FWHM, which means that only one of these parameters is required for fatigue prediction.

W-EDM and AWJM have similar fatigue life, with W-EDM only 18% lower, which is connected to the negative aspect of tensile stresses for W-EDM and embedded particles for AWJM even though this surface has relatively high compressive stresses.

The most prominent models suggested to predict the fatigue are decision tree and PLS, with the following pros and cons.

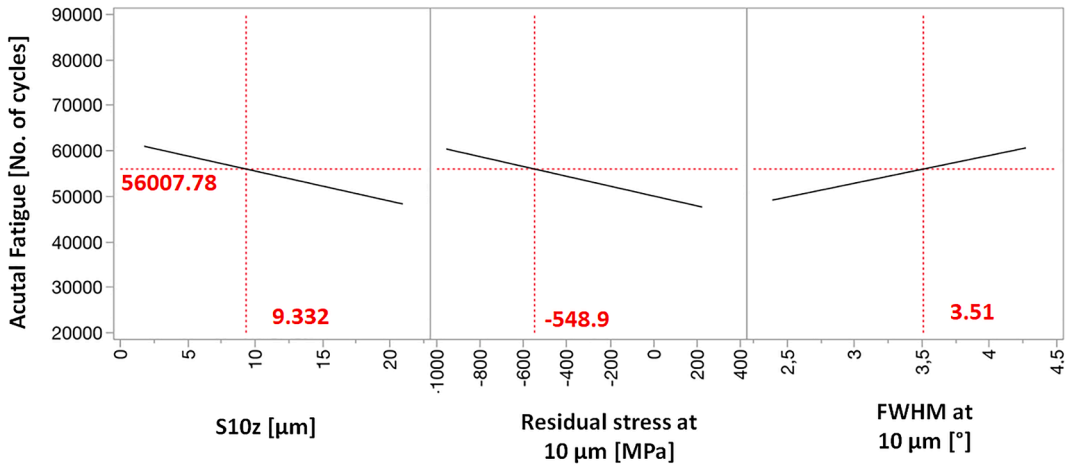

Fig. 10. Resulting fatigue for the prediction profiles for each response.

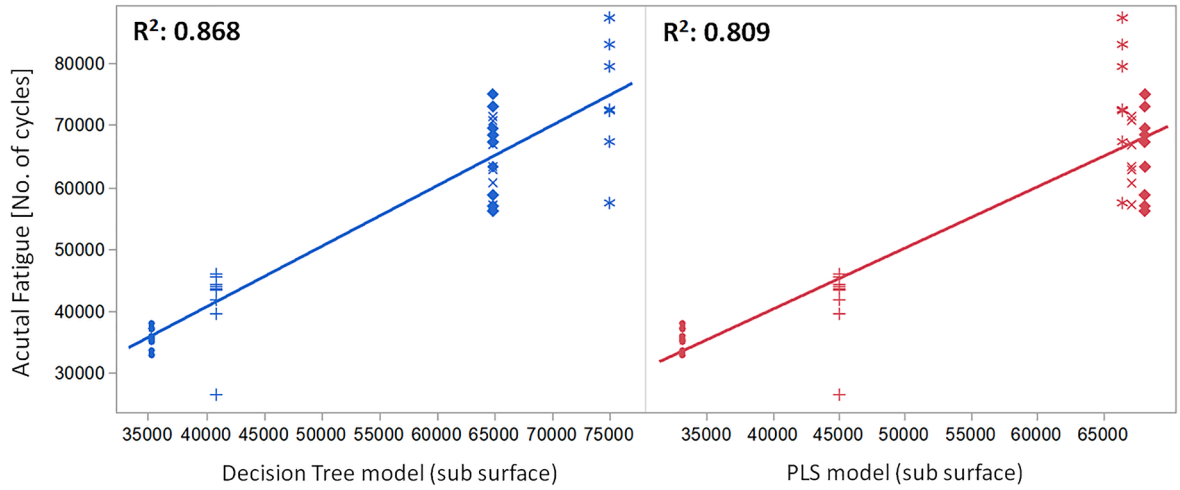

Fig. 11. Comparison between actual and prediction models for the two models, Decision tree (left) and PLS model (Right).

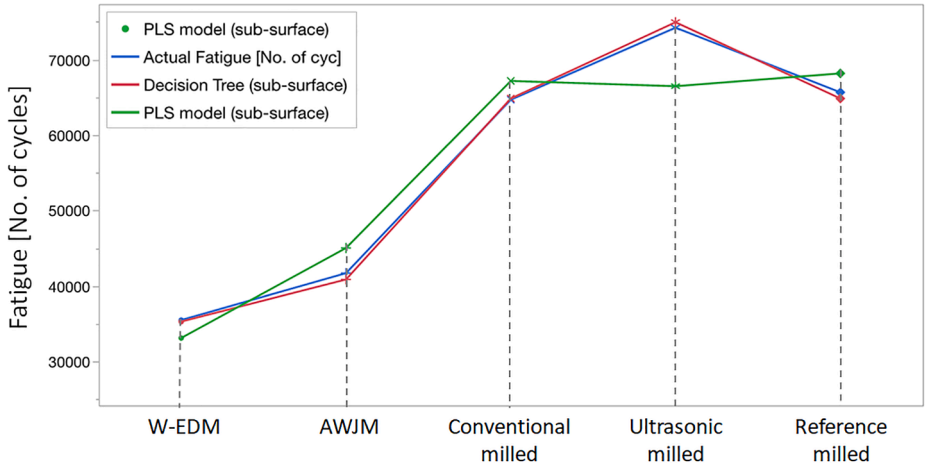

Fig. 12. Comparison of the perdition per machining method for the two models.

- Decision tree requires more training data, at distinct levels, to predict with high resolution. In this study it managed to separate the different machining methods used at one distinct setting each. Tests on several different levels with each method needs to be conducted in order to refine the model.
- PLS need more observations on order to secure a robust prediction. In this investigation only one observation per method was used which limits the model's ability to predict accurately, assuming interactions spanning the entire experimental range.

Table 8
Assessed fatigue results based on the two models.

Machining method	Actual Fatigue [No. of cycles]	Decision Tree (Sub surface)	Rel diff Decision tree [%]	PLS Model (Sub surface)	Rel diff PLS [%]
W-EDM	35,505	35,304	−0.57	33,134	−6.68
AWJM	41,719	40,886	−2.00	45,052	7.99
Conventional milled	64,699	64,861	0.25	67,181	3.84
Ultrasonic milled	74,233	74,962	0.98	66,491	−10.43
Reference milled	65,682	64,861	−1.25	68,182	3.81

Ethics declaration

This research did not involve Human Participants and/or Animals.

Declaration of Competing Interest

The authors declare that they have no known competing financial interests or personal relationships that could have appeared to influence the work reported in this paper.

Acknowledgement

The results from this work was granted from the research project G5Demo-2 [2013-04666] and SWE DEMO MOTOR [2015-06047] financed by VINNOVA, Sweden's innovation agency. Special thanks to GKN Aerospace Sweden AB. The authors also would like to thank the KK-foundation and the SiCoMaP research school.

References

[1] Zahavi E, Torbilo V, Press S. Fatigue design: life expectancy of machine parts. Taylor & Francis; 1996.
[2] Javidi A, Rieger U, Eichlseder W. The effect of machining on the surface integrity and fatigue life. Int J Fatigue 2008;30:2050–5. https://doi.org/10.1016/j.ijfatigue.2008.01.005.
[3] Totten G, Howes M, Inoue T. Handbook of residual stresses and deformation of steel. 1st ed. ASM International; 2002.
[4] Holmberg J, Berglund J, Wretland A, Beno T. Evaluation of surface integrity after high energy machining with EDM, laser beam machining and abrasive water jet machining of alloy 718. Int J Adv Manuf Technol 2018. https://doi.org/10.1007/s00170-018-2697-z.
[5] Suárez A, Veiga F, Polvorosa R, Artaza T, Holmberg J, de Lacalle LNL, et al. Surface integrity and fatigue of non-conventional machined Alloy 718. J Manuf Processes 2019;48:44–50. https://doi.org/10.1016/j.jmapro.2019.09.041.
[6] Koster WP, Fritz LJ. Surface Integrity in Conventional Machining 1970: V01BT02A033. https://doi.org/10.1115/70-GT-100.
[7] Chan KS. Roles of microstructure in fatigue crack initiation. Int J Fatigue 2010;32:1428–47. https://doi.org/10.1016/j.ijfatigue.2009.10.005.
[8] Wang X, Huang C, Zou B, Liu G, Zhu H, Wang J. Experimental study of surface integrity and fatigue life in the face milling of inconel 718. Front Mech Eng 2018;13:243–50. https://doi.org/10.1007/s11465-018-0479-9.
[9] Uthayakumar M, Khan MA, Kumaran ST, Slota A, Zajac J. Machinability of nickel-based superalloy by abrasive water jet machining. Mater Manuf Processes 2016;31:1733–9. https://doi.org/10.1080/10426914.2015.1103859.
[10] Kong MC, Axinte D, Voice W. Aspects of material removal mechanism in plain waterjet milling on gamma titanium aluminide. J Mater Process Technol 2010;210:573–84. https://doi.org/10.1016/j.jmatprotec.2009.11.009.
[11] Kong MC, Axinte D, Voice W. Challenges in using waterjet machining of NiTi shape memory alloys: an analysis of controlled-depth milling. J Mater Process Technol 2011;211:959–71. https://doi.org/10.1016/j.jmatprotec.2010.12.015.
[12] Huang L, Kinnell P, Shipway PH. Parametric effects on grit embedment and surface morphology in an innovative hybrid waterjet cleaning process for alpha case removal from titanium alloys. Procedia CIRP 2013;6:594–9. https://doi.org/10.1016/j.procir.2013.03.077.
[13] Rivero A, Alberdi A, Artaza T, Mendia L, Lamikiz A. Surface properties and fatigue failure analysis of alloy 718 surfaces milled by abrasive and plain waterjet. Int J Adv Manuf Technol 2018;94:2929–38. https://doi.org/10.1007/s00170-017-0979-5.
[14] Boud F, Loo LF, Kinnell PK. The impact of plain waterjet machining on the surface integrity of aluminium 7475. Procedia CIRP 2014;13:382–6. https://doi.org/10.1016/j.procir.2014.04.065.
[15] Thomas DJ. Characteristics of abrasive waterjet cut-edges and the affect on formability and fatigue performance of high strength steels. J Manuf Processes 2009;11:97–105. https://doi.org/10.1016/j.jmapro.2009.12.001.
[16] Ayesta I, Izquierdo B, Flaño O, Sánchez JA, Albizuri J, Avilés R. Influence of the WEDM process on the fatigue behavior of Inconel® 718. Int J Fatigue 2016;92, Part 1:220–33. https://doi.org/10.1016/j.ijfatigue.2016.07.011.
[17] Mine MA. Cumulative damage in fatigue. J Appl Mech 1945;12:A159–64.
[18] Ince A, Glinka G. A generalized fatigue damage parameter for multiaxial fatigue life prediction under proportional and non-proportional loadings. Int J Fatigue 2014;62:34–41. https://doi.org/10.1016/j.ijfatigue.2013.10.007.
[19] Santecchia E, Hamouda AMS, Musharavati F, Zalnezhad E, Cabibbo M, El Mehtedi M, et al. A review on fatigue life prediction methods for metals. Adv Mater Sci Eng 2016;2016:9573524. https://doi.org/10.1155/2016/9573524.
[20] Xiao WL, Chen HB, Yin Y. Effects of surface roughness on the fatigue life of alloy steel. Key Eng Mater 2013;525–526:417–20. https://doi.org/10.4028/www.scientific.net/KEM.525-526.417.
[21] Sanaei N, Fatemi A. Analysis of the effect of surface roughness on fatigue performance of powder bed fusion additive manufactured metals. Theor Appl Fract Mech 2020;108:102638. https://doi.org/10.1016/j.tafmec.2020.102638.
[22] Zabala A, Blunt L, Tato W, Aginagalde A, Gomez X, Llavori I. The use of areal surface topography characterisation in relation to fatigue performance. MATEC Web Conf 2018;165. https://doi.org/10.1051/matecconf/201816514013.
[23] Fernández Pariente I, Guagliano M. About the role of residual stresses and surface work hardening on fatigue ΔKth of a nitrided and shot peened low-alloy steel. Surf Coat Technol 2008;202:3072–80. https://doi.org/10.1016/j.surfcoat.2007.11.015.
[24] Zhang Z, Qi Y, Delagnes D, Bernhart G. Microstructure variation and hardness diminution during low cycle fatigue of 55NiCrMoV7 steel. J Iron Steel Res Int 2007;14:68–73. https://doi.org/10.1016/S1006-706X(07)60093-4.
[25] Vashista M, Paul S. Correlation between full width at half maximum (FWHM) of XRD peak with residual stress on ground surfaces. Phil Mag 2012;92:4194–204. https://doi.org/10.1080/14786435.2012.704429.
[26] Rai S, Choudhary BK, Jayakumar T, Rao KBS, Raj B. Characterization of low cycle fatigue damage in 9Cr–1Mo ferritic steel using X-ray diffraction technique. Int J Press Vessels Pip 1999;76:275–81. https://doi.org/10.1016/S0308-0161(98)00140-9.
[27] Shintani T, Murata Y. Evaluation of the dislocation density and dislocation character in cold rolled Type 304 steel determined by profile analysis of X-ray diffraction. Acta Mater 2011;59:4314–22. https://doi.org/10.1016/j.actamat.2011.03.055.
[28] Marty B, Guedou JY, Gergaud P, Lebrun JL. Recrystallization and work-hardening prediction during forging process of Inconel 718; The Minerals, Metals & Materials Society; 1997.
[29] Quesnel DJ, Meshii M, Cohen JB. Residual stresses in high strength low alloy steel during low cycle fatigue. Mater Sci Eng 1978;36:207–15. https://doi.org/10.1016/0025-5416(78)90073-3.
[30] Goto T, Konishi T, Haruki N, Ikuno T, Yamamoto M. Fatigue life assessment of high-temperature Cr-Mo-V Rotors by X-ray Diffraction. X-ray diffraction studies on the deformation and fracture of solids. Oxford: Elsevier; 1993. p. 283–99.
[31] Pinheiro B, Lesage J, Pasqualino I, Benseddiq N. Assessment of Fatigue Damage Initiation in Oil and Gas Steel Pipes 2011:35–44. https://doi.org/10.1115/OMAE2011-49044.
[32] Pinheiro B, Lesage J, Pasqualino I, Benseddiq N, Bemporad E. Toward a Fatigue Life Assessment of Steel Pipes Based on X-Ray Diffraction Measurements 2015: V05BT04A027. https://doi.org/10.1115/OMAE2015-42277.
[33] Fujimura N, Oguma H, Nakamura T. Damage Assessment on Low Cycle Fatigue Properties of Cyclic Pre-Strained Austenitic Stainless Steel 2011:1061–7. https://doi.org/10.1115/PVP2011-57832.
[34] Noyan IC, Cohen JB. Residual stress measurement by diffraction and interpretation. 1987 ed. Springer-Verlag New York Inc.; 1987.
[35] SAE International. Residual stress measurement by X-ray diffraction, HS-784. vol. 2003 Edition. SAE International; n.d.
[36] European Commitee for Standardization. EN 15305:2008 E, Non-destructive Testing – Test Method for Residual Stress analysis by X-ray Diffraction; 2008.
[37] Mathlock BS, Snoha DJ, Grendahl SM. Using XRD elastic and plastic strain data to evaluate the effectiveness of different cold-working techniques in aerospace materials. In: Advances in X-Ray Analysis (AXA), Proceedings Denver X-Ray Conference, vol. 52; 2008.
[38] Prevéy PS. The measurement of subsurface residual stress and cold work distributions in nickel base alloys. In: Proceedings of ASM's Conference on Residual Stress– in Design, Process, and Materials Selection 1987;Cincinnati, Ohio, USA, 27-29 April 1987, pp. 11–9.
[39] International Organisation for Standarization. ISO 25178-2:2012, Geometrical product specifications (GPS) – Surface texture: Areal – Part 2: Terms, definitions and surface texture parameters; 2012.
[40] Holmberg J, Wretland A, Berglund J, Beno T. A detailed investigation of residual stresses after milling Inconel 718 using typical production parameters for assessment of affected depth. Mater Today Commun 2020;24:100958. https://doi.org/10.1016/j.mtcomm.2020.100958.
[41] Holmberg J, Wretland A, Berglund J, Beno T. Selection of milling strategy based on surface integrity investigations of highly deformed Alloy 718 after ceramic and

cemented carbide milling. J Manuf Processes 2020;58:193–207. https://doi.org/10.1016/j.jmapro.2020.08010.

[42] Maiya PS, Busch DE. Effect of surface roughness on low-cycle fatigue behavior of type 304 stainless steel. Metall Trans A 1975;6:1761. https://doi.org/10.1007/BF02642305.

[43] Klotz T, Miao HY, Bianchetti C, Lévesque M, Brochu M. Analytical fatigue life prediction of shot peened Inconel 718. Int J Fatigue 2018;113:204–21. https://doi.org/10.1016/j.ijfatigue.2018.04.011.